



UNIVERSITY OF LEEDS

This is a repository copy of *A novel model predictive control scheme based observer for working conditions and reconditioning monitoring of Zinc-Nickel single flow batteries*.

White Rose Research Online URL for this paper:

<https://eprints.whiterose.ac.uk/153516/>

Version: Accepted Version

Article:

Li, S, Li, K, Xiao, E et al. (3 more authors) (2020) A novel model predictive control scheme based observer for working conditions and reconditioning monitoring of Zinc-Nickel single flow batteries. *Journal of Power Sources*, 445. 227282. ISSN 0378-7753

<https://doi.org/10.1016/j.jpowsour.2019.227282>

Crown Copyright © 2019 Published by Elsevier B.V. All rights reserved. This manuscript version is made available under the CC-BY-NC-ND 4.0 license
<http://creativecommons.org/licenses/by-nc-nd/4.0/>.

Reuse

This article is distributed under the terms of the Creative Commons Attribution-NonCommercial-NoDerivs (CC BY-NC-ND) licence. This licence only allows you to download this work and share it with others as long as you credit the authors, but you can't change the article in any way or use it commercially. More information and the full terms of the licence here: <https://creativecommons.org/licenses/>

Takedown

If you consider content in White Rose Research Online to be in breach of UK law, please notify us by emailing eprints@whiterose.ac.uk including the URL of the record and the reason for the withdrawal request.



eprints@whiterose.ac.uk
<https://eprints.whiterose.ac.uk/>

A Novel Model Predictive Control Scheme Based Observer for Working Conditions and Reconditioning Monitoring of Zinc-Nickel Single Flow Batteries

Shawn LI^a, Kang LI^{a,*}, Evan XIAO^b, Rui XIONG^{c,**}, Jianhua ZHANG^d, Peter FISCHER^e

^a*School of Electronic and Electric Engineering, University of Leeds, LS2 9JT, UK*

^b*Evan XIAO was with the Tepper School of Business, Carnegie Mellon University, Pittsburgh, PA 15213, USA*

^c*National Engineering Laboratory for Electric Vehicles, School of Mechanical Engineering, Beijing Institute of Technology, Beijing 100081, China*

^d*The State Key Laboratory of Alternate Electrical Power System with Renewable Energy Sources, North China Electric Power University, Beijing 102206, China*

^e*Fraunhofer-Institute for Chemical Technology, Department of Applied Electrochemistry, Joseph-von-Fraunhofer-Strasse 7, D-76327 Pfanztal, Germany*

Abstract

Zinc-nickel single flow batteries (ZNBs) have been demonstrated as a promising alternative to lithium batteries for next generation grid-tied energy storage. However, due to the dendritic growth, the **monitoring of working conditions** in terms of the state of charge (SoC) and battery capacity is intractable. Although longer lifespan can be **achieved through** the periodic reconditioning maintenance, there is no mature method to identify the moment of reconditioning. Model predictive control (MPC) is a popular optimization paradigm in the process control. By incorporating the merits of model predictive control, this work presents a novel model predictive control based observer (MPCO) for the working conditions monitoring and reconditioning identification. Strong evidence from substantial experiments and simulations manifests the convergence, robustness, effectiveness and generality of the proposed method. The competitiveness is demonstrated by analytical comparisons against other three estimators. In this regard, the relationships of the proposed observer with other estimators are summarized briefly. At last, an indicator **based on** the capacity changes is proposed to judge the timing of reconditioning.

Keywords: Redox flow batteries, Zinc-Nickel Single Flow Batteries, State of Charge estimation, Capacity estimation, Reconditioning, Model predictive control, Observer

1. Introduction

The energy storage applications integrated into the power grid promote high penetration of renewable sources, in particular, the wind and solar power [1, 2, 3]. Long-life rechargeable batteries **have less** geomorphic restraints [4], hence can flexibly address the sporadic availability issues of the renewable energy resource. In this regard, the scaled-up battery systems are routinely settled alongside the renewable energy resource to improve the power quality and system reliability [5]. Redox flow battery (RFB) is one of the most promising grid-tied energy storage technologies in the marketplace. **Unlike lithium batteries**, a typical individual RFB system is relieved from the constraint between the storage capacity and the rated power by separating the electrolyte reservoir and **the battery stacks** [4, 5, 6, 7]. Because of the partial re-usability of battery materials [5], the disposal of redox couples is more effective and economical. Unlike lithium batteries, the aqueous electrolyte is widely used in RFB, leading to small solubility of the active species in the aqueous electrolyte, which restrains the electrolyte conditions and averages current material density. As a consequence, though the concept of RFB was proposed in 1974 by Thaller [7], only the all-vanadium flow batteries (VFBs) pioneered by Skyllas-Kazacos et al [8] are commercially available. However, the energy density of VFBs is still limited by the intrinsically low solubility of vanadium. Other challenges [4, 5] such as energy wastes, extra costs on membranes, and high system complexities have arisen, because the electrolyte is separated into two reservoirs.

As alternatives to the lithium batteries and other RFB counterparts, an innovative RFB system based on nickel and zinc redox couples was first proposed [9]. The theoretical capacity and energy ratio of Zinc-Nickel single flow batteries (ZNBs) are higher than other RFB counterparts. The intrinsic electromotive force is above $1.72V$ [10], which is much higher than VFBs ($1.20V$) [8], leading to an improved specific energy (more than $85Wh/kg$) [9, 11].

*Corresponding author

**Corresponding author

Email addresses: elxli@leeds.ac.uk (Shawn LI), k.li1@leeds.ac.uk (Kang LI),
rxiong@bit.edu.cn (Rui XIONG)

The nominal voltage maintains up to 1.60V throughout the discharging period [9, 11]. The discharging voltage is relatively stable at broad ranges of current rates. Moreover, the aqueous electrolyte exhibits distinguishing stability and non-toxicity under over-charging and over-discharging scenarios [11]. An interesting feature of ZNBs is the membrane-free system, thus the expensive membranes are **not needed in** the system design leading to cost-saving and **simplified manufacturing** [9]. Whereas, the viability of a commercial nickel zinc battery has been hindered by the well-known phenomena of dendrite formation and zinc morphology variation over time. Two fundamental culprits are the swelling of the nickel electrode (cathode) resulted from the uneven current distribution, and the poor cycling characteristics of the zinc electrode (anode) because of the growth of zinc dendrites [12]. Throughout the charging phase, the active materials are redistributed leading to a nonlinear distribution, so that redox reaction is far from the equilibrium status. As a result, a concentrated layer of zincate boundary is grown around the surface of the zinc electrode, resulting in the appearance of dendritic zinc depositions [13, 10]. Once dendrite is formed, due to the higher current density at the tips than other locations, **the dendrites growth is even more aggressive** [14, 15]. Eventually, battery failures can be observed, such as internal short circuits, cell housing damage, capacity deterioration, unreliable cell performance and etc. In this regard, number of studies focus on **how to suppress the zinc dendrite formation** [10, 12, 13, 14, 15]. Non-organic and organic additives [16] have been added in the electrolyte and electrode. However, it is time-consuming to find a proper additive based on the extensive experiments. On the other hand, surface modification techniques have been investigated by other research groups, to seek positive long-term effects on cycling performance. Synthesized ZnO was used by [12, 14, 15] to control the shape of anode [15]. There is considerable diversity in the structure of the synthesized ZnO , so that substantial experiments are needed before the commercialization. Besides, a compact zinc morphology is achievable through limiting the applied current densities [13], which is **however difficult to implement in** practical battery applications.

From the practical perspective, periodic reconditioning was thus introduced in [13, 17]. After a number of cycles, ZNBs will stop to conduct the reconditioning maintenance, i.e.

a slowly trickling discharging cycle. In this way, the undissolved zinc depositions can be stripped off from the surface of electrode. However, the unstable performance of ZNBs has not been addressed. Specifically, two challenges are prevailing. One is that the unpredictable zinc dendrites growth and residual uneven zinc morphology lead to the variations in capacity values after each discharging cycle, resulting in shifting of State of Charge (SoC) estimation. Unlike other counterparts, the SoC estimation of ZNBs has turned out to be inaccurate and unreliable. The other difficulty is to determine the moment of reconditioning maintenance. In this work, a novel framework of the SoC observer is introduced by the inspiration of the model predictive control (MPC) scheme. MPC is a process control strategy developed in the 1970s [18]. The systematic mathematical model is used to assess the influence of the current control actions on the plant performance in the future [19]. The most remarkable advantage of MPC is multiple constraints handling [20]. Moreover, the optimum solution will be solved at each time step over a finite prediction horizon [21]. Analogous to the MPC scheme, in this note, the electrochemical constraints against the internal states estimates in terms of the polarization voltage and SoC are imposed based on a first-order electrical equivalent model (ECM). On the other hand, the implantation of rolling-horizon (window) technique improves the precision of capacity estimation. Therefore, the influences of capacity fluctuations are attenuated effectively by the proposed method. In addition, the degree of capacity degradation can be treated as an indicator to trigger the reconditioning maintenance. Experiments have been performed on a handmade bench-scale ZNBs to affirm the extraordinary efficiency and accuracy of the proposed MPC based observer (MPCO).

The major contribution of this paper is to design a nonlinear observer framework for SoC estimation of ZNBs based on the MPC scheme. The mechanism to conduct the reconditioning operation has then been **proposed** according to the tendency of the capacity degradation. Besides, this work analytically compares the performances with the other three state-of-the-art SoC estimators and briefly summarises the rationales behind them, encompassing Extended Kalman Filter (EKF), H -Infinity Filter and Sliding Mode Observer (SMO).

2. Modelling and identification

According to various requirements of the modelling accuracy and practical applications, many attempts to reproduce the electric dynamics of the battery have been reviewed [22]. The widely accepted methods are the electrochemical model and equivalent circuit model (ECM) [21]. The electrochemical model provides more **accurate** results at the expense of higher **computational** complexity and numerical instability. It is thus often adopted in the battery design process to investigate the material influences on internal states based on the specific parameters with the prescribed boundaries. Due to its complicated structure, the electrochemical model does not work well for online applications. On the other hand, ECM utilises different electrical parameters in terms of the resistor, the capacitor, and the voltage source to depict the battery nonlinear behaviours. On the basis of the recent studies of the major ECM applications [22], the first-order resistor-capacitor (RC) has been demonstrated as a suitable tool for online applications as it represents a trade-off **model** between complexity and accuracy.

2.1. Equivalent circuit model

A typical first-order ECM is considered in this work as illustrated in Fig.1. Throughout the charging/discharging phases, R_s is the encountered ohmic resistance resulting in the energy losses at the electrodes and electrolytes. It is noted that even at the same SoC level, R_s is influenced by the ambient temperature and the ageing modes. The parallel RC branch is employed to model the ZNBs transient responses and relaxation effects that appear during and out of the cycles respectively, due to the existence of the activation polarization and concentration polarization voltage (V_p). In this regard, R_p and C_p represents the polarisation resistance and capacitance, respectively. Due to the above influences, once the terminal current I_L stops loading into the ZNBs, the terminal voltage signals V_t will slowly converge to its equilibrium, denoted as open circuit voltage (OCV) V_{oc} . At the efforts of the auxiliary flow system (pump), the circulating electrolyte will effectively attenuate the polarization voltage V_p and progressively facilitate the process of equilibrium [9].

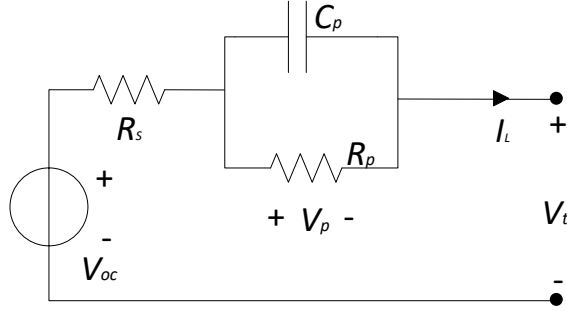


Figure 1: Schematic diagram of the first-order ECM

Apart from the above simple linear model, the statically monotonous correlation between V_{oc} and SoC is the routine benchmark in the process of battery modelling. However, this relationship is intrinsically nonlinear and can be obtained from the experimental data only. Therefore, the incremental OCV tests (IO) [23] are conducted to formulate the SoC-OCV table. In this regard, the constant current constant voltage (CCCV) charging profile is loaded to the ZNBs to reach a fully charged status. Then, successive discharge segments **in the form of** pulse current are performed to drain up the capacity of ZNBs. Throughout the entire cycle, the SoC values are recorded by high precision current sensors based on the coulomb counting (CC) method. Meanwhile, the OCV values are logged at the end of each discharging SoC interval. Finally, the SoC-OCV relationship is characterized by averaging three current profiles in terms of $0.5C(1.85A)$, $1C(3.70A)$, and $1.5C(5.55A)$. In this work, the SoC-OCV relationship is modeled as a fifth-order polynomial [24]:

$$V_{oc} = f(SoC) = \sum_{j=0}^p \rho_j SoC^j \quad (1)$$

where p is the selected order (which is 5 in this work) of least square (LS) error curve fitting technique; ρ_j are the polynomial coefficients to fit the nonlinear correlation. The rationale and justification of the above method are elaborated in [24]. On the other hand, due to the merits of the flowing electrolyte, the generated heat will be transmitted outside by the circulating electrolyte while dissipating away fleetly. Therefore, the effects of temperature on SoC-OCV table is negligible.

2.2. Online model parameter identification

The dynamic process of the chemical reactions is also associated with the influences of the ambient temperature and aging modes. Besides, ZNB is a slowly time-varying system. In order to best model the battery process, the parameters **have to be updated regularly** to adjust to **process dynamics** [24]. In this paper, the recursive least square (RLS) with a fixed user-defined forgetting factor $\lambda = 0.98$ is adopted to identify the model parameters online while considering the **effects of the environment, aging evolution and other unmodeled dynamics**.

Assuming the positive sign of current is for discharge, and vice versa. Based on the Kirchhoff laws and the principle of the RC circuit, the electrical model is governed by the following ordinary differential equations (ODE):

$$C_p \frac{dV_p}{dt} + \frac{V_p}{R_p} = I_L \quad (2)$$

$$V_t = V_{OC} - V_p - I_L R_s \quad (3)$$

Followed on, the one time step discretization of Eq. (2) is of the expression:

$$V_p(t) = e^{-\frac{\Delta t_s}{R_p C_p}} V_k(t - \Delta t_s) + \left(1 - e^{-\frac{\Delta t_s}{R_p C_p}}\right) R_p I_L(t - \Delta t_s) \quad (4)$$

where the time interval Δt_s is the sample rate and is fixed in the whole experiments. Assuming 0 is the starting point of the discretized series, denote $V_p(k) = V_p(k\Delta t_s)$. Analogous to V_p , the similar definitions are applied to V_{OC} , V_t , and I_L . Therefore, Eq. (4) can be rewritten in a neat format:

$$V_p(k) = e^{-\frac{\Delta t_s}{R_p C_p}} V_p(k-1) + \left(1 - e^{-\frac{\Delta t_s}{R_p C_p}}\right) R_p I_L(k-1) \quad (5)$$

Based on Eq.(3), by substituting $V_p = V_{OC} - V_t - I_L R_s$ in Eq.(5), the terminal voltage V_t is obtained as follows:

$$\begin{aligned} V_t(k) &= \beta V_t(k-1) - R_s I_L(k) + (\beta \cdot R_s - (1 - \beta) R_p) I_L(k-1) \\ &\quad + (V_{OC}(k) - \beta V_{OC}(k-1)), \end{aligned} \quad (6)$$

where $\beta = e^{-\frac{\Delta t_s}{R_p C_p}}$. During the ZNBs cycling, the V_{OC} is a slowly varying state opposite to the terminal voltage V_t , where OCV variations are subtle between two neighbouring sample points. Thereby, the one-time step difference is taken to remove the influence of OCV in the process of the parameter identification. The differential voltage is drawn as follows:

$$\begin{aligned} \Delta V_t(k) = & \beta \Delta V_t(k-1) - R_s \Delta I_L(k) + (\beta \cdot R_s - (1-\beta)R_p) \Delta I_L(k-1) \\ & + (\Delta V_{OC}(k) - \beta \Delta V_{OC}(k-1)), \end{aligned} \quad (7)$$

in this regard, Eq.(7) can be regressively expressed in a linear form:

$$y(k) = \theta^T(k) \phi(k) + e(k), \quad (8)$$

where

$$\begin{aligned} y(k) = \Delta V_t(k), \quad \theta(k) = \boldsymbol{\alpha} = [\alpha_1, \alpha_2, \alpha_3]^T = [\beta, -R_s, \beta \cdot R_s - (1-\beta)R_p]^T, \\ \phi(k) = [\Delta V_t(k-1), \Delta I_L(k), \Delta I_L(k-1)]^T, \quad e(k) = \Delta V_{OC}(k) - \alpha_1 \Delta V_{OC}(k-1). \end{aligned}$$

and $e(k)$ is assumed as the error term in this regression procedure. Due to the feature of slowly changing OCV, as long as the sample rate is fast enough, the error terms are negligible. Therefore, the RLS method is applied to Eq.(8) to estimate the slowly time-varying parameters $\theta(k)$ under different working environments. The process of RLS method can then be summarized as follows.

$$y(k) = \theta(k)^T \cdot \phi(k) + \varepsilon(k) \quad (9)$$

$$\varepsilon(k) = E(k) - \theta(k-1)^T \cdot \phi(k) \quad (10)$$

$$K(k) = \frac{P(k-1)\phi(k)}{\lambda + \phi_k^T P(k-1)\phi(k)} \quad (11)$$

$$P(k) = \lambda^{-1} (P(k-1) - K(k)\phi(k)^T P(k-1)) \quad (12)$$

$$\theta(k) = \theta(k-1) + K(k)e(k) \quad (13)$$

where $y(k)$ is the measured voltage $V_t(k)$ signals. Besides, $\phi(k)$ and $\theta(k)$ are the model input signals and the estimated parameter respectively. $P(k)$ is the covariance matrix used to update the parameters. A fixed user-defined forgetting factor λ to scale the contributions

of previous samples to the covariance matrix. The parameters $\hat{\theta}(k)$ of the regression model can thus be solved at each sample point. Afterwards, the parameters $[\hat{R}_s, \hat{R}_p, \hat{C}_p]^T$ of the ECM can be then calculated reversely:

$$\begin{aligned}\hat{R}_s &= -\hat{\alpha}_2, & \hat{\beta} &= \hat{\alpha}_1, \\ \hat{R}_p &= \frac{\hat{\beta} \cdot \hat{R}_s - \hat{\alpha}_3}{1 - \hat{\beta}} = \frac{-\hat{\alpha}_1 \hat{\alpha}_2 - \hat{\alpha}_3}{1 - \hat{\alpha}_1}, \\ \hat{C}_p &= -\frac{\Delta t_s}{\hat{R}_p \log(\hat{\beta})} = \frac{\Delta t_s \cdot (1 - \hat{\alpha}_1)}{(\hat{\alpha}_1 \hat{\alpha}_2 + \hat{\alpha}_3) \log(\hat{\alpha}_1)}.\end{aligned}$$

3. SoC Observer and Reconditioning Indicator

The closed-loop online SoC estimation approach plays an indispensable role in both academia and industry, thus raising growing attentions. In particular, Extended Kalman filtering (EKF) [25] and its variants have been integrated into ECM modeling process in the recent years. In order to compensate for the over-potential dynamics and keep the intact nonlinearity of the battery model, H -infinity [26] method and particle filter (PF) [27] are adopted respectively as the improvements of EKF. Apart from the above filters, other implementations such as sliding-mode observer (SMO) [28], nonlinear geometric observer [29], and Luenberger-type observers [30] are also proposed in line with the control paradigms and theories.

3.1. MPC based Observer Design

MPC is a powerful optimization controller taking all the model-based process interactions into consideration, where the control action at each sampling point will be determined by solving the finite horizon optimization in real time. The successfully widespread deployment of MPC in the industrial applications has confirmed its effectiveness. In practice, nearly every application imposes constraints. MPC is one of few suitable control methods to advantageously handle the constraints on manipulated variables and states simultaneously. In this paper, inspired by the control paradigm of MPC [18] and SMO [28], a novel MPC-based SoC observer (MPCO) is introduced in this section. It is known that the outputs of

ECM are not **accurate** matches to the real measurements. The errors from measurements, discretization process, and parameter identification in RLS have to be compensated by the proposed SoC observer. According to Eq.(5), the two-dimensional state equations along with small friction terms are formulated as follows:

$$\begin{cases} SoC(k) = SoC(k-1) - \frac{\eta \Delta t_s}{Q} I_L(k-1) + f_1(k-1) \\ V_p(k) = e^{-\frac{\Delta t_s}{R_p C_p}} V_p(k-1) + \left(1 - e^{-\frac{\Delta t_s}{R_p C_p}}\right) R_p I_L(k-1) + f_2(k-1) \end{cases} \quad (14)$$

where Q is the capacity of ZNBs, whilst f_1 and f_2 stand for the errors not only from measurements, modelling, and discretization, but also from the time-varying parameters identified in RLS. Analogous to other observer/filter designs, the terminal voltage V_t is the main focus of measurement equation:

$$V_t(k) = f(SoC(k)) - V_p(k) - R_s I_L(k) + f_3(k) \quad (15)$$

where f is the pre-calibrated SoC-OCV table expressed as $V_{OC} = f(SoC)$. Herein, the $f_1(k)$ and $f_2(k)$ are systematic frictions. In coincidence with the framework of the state equations Eq.(14), $f_3(k)$ represents measurement equation friction. Assuming the systematic frictions and measurement friction are independent, and thus are of the expressions as:

$$\begin{bmatrix} f_1(k) \\ f_2(k) \end{bmatrix} \sim N(0, \Sigma), \quad f_3(k) \sim N(0, \sigma^2) \quad (16)$$

where Σ and σ are error covariance matrix and the standard deviation, respectively, which are used to solve control law in the followed-on process. Denotes $\mathbf{x}(k) = [SoC(k), V_p(k)]^T$ and thus the state vector $\mathbf{X}(k)$ and measurement vector $\mathbf{Y}(k)$ for n steps are derived as: ‘

$$\mathbf{X}(k) = \begin{bmatrix} \mathbf{x}(k-n+1) \\ \mathbf{x}(k-n+2) \\ \vdots \\ \mathbf{x}(k) \end{bmatrix}, \quad \mathbf{Y}(k) = \begin{bmatrix} V_t(k-n+1) \\ V_t(k-n+2) \\ \vdots \\ V_t(k) \end{bmatrix} \quad (17)$$

where n is the decision window in the MPCO. Therefore, a neat state equation is written as:

$$\mathbf{X}(k+1) = A_k \cdot \mathbf{X}(k) + B_k \cdot \mathbf{u}(k) + \mathbf{f}(k) \quad (18)$$

where

$$\begin{aligned}
A_k &= \begin{bmatrix} 0 & I_2 & 0 & \cdots & 0 \\ 0 & 0 & I_2 & \cdots & 0 \\ \vdots & \vdots & \vdots & \vdots & \vdots \\ 0 & 0 & 0 & \cdots & I_2 \\ 0 & 0 & 0 & \cdots & A \end{bmatrix}, & B_k &= \begin{bmatrix} 0 & 0 & 0 & \cdots & 0 \\ 0 & 0 & 0 & \cdots & 0 \\ \vdots & \vdots & \vdots & \vdots & \vdots \\ 0 & 0 & 0 & \cdots & 0 \\ 0 & 0 & 0 & \cdots & B \end{bmatrix}, & \mathbf{u}(k) &= \begin{bmatrix} I_L(k-n+1) \\ I_L(k-n+2) \\ \vdots \\ I_L(k-1) \\ I_L(k) \end{bmatrix} \\
\mathbf{f}(k) &= \begin{bmatrix} 0 \\ 0 \\ \vdots \\ 0 \\ \mathbf{f}(k) \end{bmatrix}, & A &= \begin{bmatrix} 1 & 0 \\ 0 & e^{-\frac{\Delta t_s}{R_p C_p}} \end{bmatrix}, & B &= \begin{bmatrix} -\frac{\eta \Delta t_s}{Q} \\ 1 - e^{-\frac{\Delta t_s}{R_p C_p}} \end{bmatrix}, & \mathbf{f}(k) &= \begin{bmatrix} f_1(k) \\ f_2(k) \end{bmatrix}
\end{aligned}$$

Suppose the posteriori-estimate $\hat{\mathbf{X}}(k)$ and the corresponding error covariance matrix $\hat{\Sigma}_k$ have been obtained after the k -th measurement. Thereby, the intermediate priori-estimate $\hat{\mathbf{X}}_-(k+1)$ in the next sample instant can be calculated as follows:

$$\hat{\mathbf{X}}_-(k+1) = A_k \cdot \hat{\mathbf{X}}(k) + B_k \cdot \mathbf{u}(k) \quad (19)$$

Afterwards, the posteriori-estimate $\hat{\mathbf{X}}(k+1)$ can be corrected by solving the control law as:

$$\hat{\mathbf{X}}(k+1) = \hat{\mathbf{x}}_-^{(n)}(k+1) + \Delta \mathbf{x}(k+1) = A_k \cdot \hat{\mathbf{X}}(k) + B_k \cdot \mathbf{u}(k) + \Delta \mathbf{x}(k+1) \quad (20)$$

where $\Delta \mathbf{x}(k+1)$ is not only the MPC control law obtained from the solution of the quadratic programming as disclosed in the following content, but also the correction to priori-estimate. The errors of the priori-estimate and posteriori-estimate are expressed as follows, respectively:

$$\begin{aligned}
\mathbf{e}_-(k+1) &= A_k \cdot \mathbf{e}(k) + \mathbf{f}(k), \\
\mathbf{e}(k+1) &= \mathbf{e}_-(k+1) - \Delta \mathbf{x}(k+1)
\end{aligned} \quad (21)$$

According to the ECM, the posteriori-estimate for $\mathbf{Y}(\hat{k} + 1)$ can be calculated:

$$\begin{aligned}
\hat{\mathbf{Y}}(k + 1) &= F(C_1 \cdot \hat{\mathbf{X}}(k + 1)) - C_2 \cdot \hat{\mathbf{X}}(k + 1) - R_s \cdot \mathbf{u}(k + 1) \\
&\approx F(C_1 \cdot \hat{\mathbf{X}}_-(k + 1)) + \left. \frac{\partial F}{\partial \mathbf{X}} \right|_{\mathbf{x}=C_1 \cdot \hat{\mathbf{X}}_-(k+1)} \cdot C_1 \cdot \Delta \mathbf{X}(k + 1) - C_2 \cdot \hat{\mathbf{X}}(k + 1) - R_s \cdot \mathbf{u}(k + 1) \\
&= F(C_1 \cdot \hat{\mathbf{X}}_-(k + 1)) - C_2 \cdot \hat{\mathbf{X}}_-(k + 1) - R_s \cdot \mathbf{u}(k + 1) + \left(\frac{\partial F}{\partial \mathbf{x}} \cdot C_1 - C_2 \right) \cdot \Delta \mathbf{x}(k + 1)
\end{aligned} \tag{22}$$

where due to the nature of recursive properties, a set of n outputs from model can be estimated. A neat form of $\mathbf{Y}(\hat{k} + 1)$ is thus reformulated as :

$$\hat{\mathbf{Y}}(k + 1) = \mathbf{y}_{k+1} + \mathbf{G} \cdot \Delta \mathbf{x}(k + 1) \tag{23}$$

where

$$\begin{aligned}
C_1 &= \text{blkdiag}\{[1 \ 0], \dots, [1 \ 0]\}, \quad C_2 = \text{blkdiag}\{[0 \ 1], \dots, [0 \ 1]\} \\
F \left(\begin{bmatrix} x_1 \\ x_2 \\ \vdots \\ x_l \end{bmatrix} \right) &= \begin{bmatrix} f(x_1) \\ f(x_2) \\ \vdots \\ f(x_l) \end{bmatrix}, \quad \frac{\partial F}{\partial \mathbf{x}} \left(\begin{bmatrix} x_1 \\ x_2 \\ \vdots \\ x_l \end{bmatrix} \right) = \text{diag}\{f'(x_1), f'(x_2), \dots, f'(x_l)\} \\
\mathbf{y}_{k+1} &= F(C_1 \cdot \hat{\mathbf{x}}_-(k + 1)) - C_2 \cdot \hat{\mathbf{x}}_-(k + 1) - R_s \cdot \mathbf{u}(k + 1), \quad \mathbf{G} = \frac{\partial F}{\partial \mathbf{x}} \cdot C_1 - C_2
\end{aligned}$$

Analogous to the control paradigm of MPC, the optimal control law i.e. the gain of the proposed MPCO, can be determined by minimizing the following cost function:

$$\begin{aligned}
J &= \|\hat{\mathbf{Y}}(k + 1) - \mathbf{Y}(k + 1)\|_{\mathcal{S}^2} + \|\mathbf{x}(k + 1) - \mathbf{x}_-(k + 1)\|_{\mathcal{R}^2} \\
&= \|\mathbf{G} \cdot \Delta \mathbf{x}(k + 1) + \mathbf{y}_{k+1} - \mathbf{Y}(k + 1)\|_{\mathcal{S}^2} + \|\Delta \mathbf{x}(k + 1)\|_{\mathcal{R}^2}
\end{aligned} \tag{24}$$

where $\hat{\mathbf{Y}}(k+1)$ is the estimated vector of future V_t given the controlled state vector $\Delta \mathbf{x}(k+1)$. On the other hand, $\mathbf{Y}(k + 1)$ is the vector of the real voltage measurements, which are considered as references. Herein, the length of the decision horizon is n . It is should be

noted that differing from the traditional framework of MPC, during each optimization step, the moment k and $n - 1$ steps ahead model outputs, which equal to the length of the decision horizon n , are compared with the real measurements. By substituting Eq.(23) into the Eq.(24), a quadratic expression is given:

$$J = \Delta \mathbf{x}(k+1)^T \cdot (\mathbf{G}^T \mathbf{S} \mathbf{G} + R) \cdot \Delta \mathbf{x}(k+1) + 2(\mathbf{y}_{k+1} - \mathbf{Y}(k+1))^T \mathbf{S} \mathbf{G} \cdot \Delta \mathbf{x}(k+1) + \mathbf{S}_y \quad (25)$$

where $\mathbf{S}_y = (\mathbf{y}_{k+1} - \mathbf{y}^{(n)}(k+1))^T \cdot \mathbf{S} \cdot (\mathbf{y}_{k+1} - \mathbf{y}^{(n)}(k+1))$. In additional, the positive definite weighting matrices R and \mathbf{S} denote the measurement error covariance and priori-estimate error covariance respectively, which can be derived as follows:

$$\mathbf{S}^{-1} = \text{diag}\{\sigma^2, \sigma^2, \dots, \sigma^2\}, \quad R^{-1} = A_k \hat{\Sigma}_k A_k^T + \text{diag}\{0, \dots, \Sigma\} \quad (26)$$

For the unconstrained optimization problem $\min_{\Delta \mathbf{x}(k+1)} J$, an analytical solution could be readily found below:

$$\Delta \mathbf{x}^*(k+1) = (\mathbf{G}^T \mathbf{S} \mathbf{G} + R)^{-1} \mathbf{G}^T \mathbf{S} (\mathbf{Y}(k+1) - \mathbf{y}_{k+1}) \stackrel{\text{def}}{=} L \cdot (\mathbf{Y}(k+1) - \mathbf{y}_{k+1}) \quad (27)$$

where L is defined to simplify equations:

$$L \stackrel{\text{def}}{=} (\mathbf{G}^T \mathbf{S} \mathbf{G} + R)^{-1} \mathbf{G}^T \mathbf{S},$$

$$I - L\mathbf{G} = I - (\mathbf{G}^T \mathbf{S} \mathbf{G} + R)^{-1} \mathbf{G}^T \mathbf{S} \mathbf{G}$$

$$= (\mathbf{G}^T \mathbf{S} \mathbf{G} + R)^{-1} R \quad (28)$$

According to matrix inverse formula, yielding:

$$(\mathbf{G}^T \mathbf{S} \mathbf{G} + R)^{-1} = R^{-1} - R^{-1} \mathbf{G}^T (\mathbf{S}^{-1} + \mathbf{G} R^{-1} \mathbf{G}^T)^{-1} \mathbf{G} R^{-1} \quad (29)$$

Hence the new covariance matrix will be expressed as:

$$\begin{aligned}
\hat{\Sigma}_{k+1}^+ &= \text{Var}[\hat{\mathbf{x}}_+(k+1)] = \text{Var}[\hat{\mathbf{x}}_-(k+1) + \Delta\mathbf{x}(k+1)] \\
&= \text{Var}[\hat{\mathbf{x}}_-(k+1) - L \cdot \mathbf{y}_{k+1} + L \cdot \mathbf{Y}(k+1)] \\
&= \text{Var}[(I - L\mathbf{G})\hat{\mathbf{x}}_-(k+1) + L \cdot \mathbf{Y}(k+1)] \\
&= (I - L\mathbf{G})R^{-1}(I - L\mathbf{G})^T + L\mathbf{S}^{-1}L^T \\
&= (\mathbf{G}^T\mathbf{S}\mathbf{G} + R)^{-1}R(\mathbf{G}^T\mathbf{S}\mathbf{G} + R)^{-1} + (\mathbf{G}^T\mathbf{S}\mathbf{G} + R)^{-1}\mathbf{G}^T\mathbf{S}\mathbf{G}(\mathbf{G}^T\mathbf{S}\mathbf{G} + R)^{-1} \\
&= (\mathbf{G}^T\mathbf{S}\mathbf{G} + R)^{-1}
\end{aligned} \tag{30}$$

For unconstrained case, calculating R is unnecessary. The only costly calculation might be $(\mathbf{S}^{-1} + \mathbf{G}R^{-1}\mathbf{G}^T)^{-1}$ in Eq. 29, which has $O(n^3)$ time complexity. However, calculating R has 7 times more complexity as the number of rows and columns of R is twice of $\mathbf{G}R^{-1}\mathbf{G}^T + \mathbf{S}^{-1}$.

3.2. Constrained formulation on SoC Observer

In order to improve the accuracy of the proposed SoC observer, a couple of constraints can be integrated into the process of the SoC estimation while keeping in line with the MPC paradigm. When incorporating the ZNBs intrinsic electrochemical characteristics into observer formulation, the controlled state variables $\Delta\mathbf{x}(k+1)$ has to be bounded within the feasible regions derived by the potential constraints. Taking polarization voltage V_p as an example, though the enlarged distance among electrodes increases the value of V_p , the circulating electrolyte can offset the distance effects to drag V_p back within $\pm 0.06V$. A faster flow rate may even further reduce the polarization voltage. Apart from V_p , the varying ranges of SoC also has to be restrained between 0 and 1. Alternatively, the SoC changes can also be limited into other ranges depending on the realistic operating conditions. Therefore, linear constraints e.g. lower and upper thresholds for SoC and V_p are integrated into the control formulation:

$$C_1\Delta\mathbf{X}(k+1) \in \left[\mathbf{s}_l - C_1\hat{\mathbf{X}}_-(k+1), \mathbf{s}_u - C_1\hat{\mathbf{X}}_-(k+1) \right] \tag{31}$$

$$C_2\Delta\mathbf{X}(k+1) \in \left[\mathbf{V}_{p,l} - C_2\hat{\mathbf{X}}_-(k+1), \mathbf{V}_{p,u} - C_2\hat{\mathbf{X}}_-(k+1) \right] \tag{32}$$

where \mathbf{s}_l and \mathbf{s}_u are the lower and upper bounds for SoC, and $\mathbf{V}_{p,l}$ and $\mathbf{V}_{p,u}$ are the lower and upper bounds for V_p . The inequalities Eq.(31) and Eq.(32) guarantee the states constraints. Then the above problem is transformed to solve a quadratic programming problem under the linear constraints. It is worth noting that in order to comply with the control theory of the MPC, the optimized solutions will be updated at each sampling point, and then only the first control signal with regard to the current instant is loaded to the actuator [31]. Analogously, merely the first line of $\Delta\mathbf{X}$ is employed as the gain value to update the state estimations. Owing to the merits of the imposed constraints, the estimated results will show a perfect match to the theoretical values. And thus the internal state estimations will converge quickly, providing a more accurate SoC estimation for the followed capacity estimation.

For the QP problem, the solution is located either in the interior of constrained area, or at the border. Therefore, two cases are discussed as follows. If the solution is in the interior, it is equivalent to the solution without constraints. And if the solution is at the borders, it means the solution is actually truncated by constraints. As the true values of the state variables lie in the constraint borders, the solution will have less error variance than no-constraint-solution, leading to less correction effect. However, the state variable is fixed at the constrained values in this case, resulting in 0 variance. In order to cope with filter system, the unconstrained covariance matrix is used to approximate constrained covariance matrix, which is smaller in theory. By doing so, similar to the scheme of H -infinity filter, the larger covariance matrix along with a less correction effect brings extra robustness to the estimation.

3.3. Time Complexity Analysis

In this section, only one window length is considered. Complexity analysis is more focused on feasibility of online estimation. Multi-window is only considered as a more accurate alternative for capacity updates after each cycle. The general method to solve quadratic programming problem with linear constraints is already sketched in Section 3.2, which is detailed as follows:

1. Suppose the problem is

$$\min_x \frac{1}{2}x^T \Gamma x + f^T x \quad (33)$$

$$s.t. \quad C_i x \leq g_i, \quad 1 \leq i \leq l \quad (34)$$

where g_i is a number and each g_i represents for a constraint.

2. As the solution will be at the border or within the border for each constraint, consider a combination of the l constraints, and solve the problem with these constraints being equal. For example, if the i_1, i_2, \dots, i_k -th constraints are selected, i.e. to solve

$$\min_x \frac{1}{2}x^T \Gamma x + f^T x \quad (35)$$

$$s.t. \quad C_i x = g_i, \quad i = i_1, i_2, \dots, i_k \quad (36)$$

The above problem can thus be easily solved using Lagrange multiplier. If the solution satisfies all constraints, it will be kept, otherwise is discarded.

3. Consider all combinations and compare the corresponding results. There will be 2^l combinations and less than 2^l valid results. Select the one with minimum cost function value as the global minimum solution.

In this paper, the state variable x is two-dimensional. There are four constraints but only 9 possible solutions are attainable, detailed as: one solution without constraints, four with one constraints, and other four with two constraints. The problem with one constraints are thus reduced to a one-dimensional quadratic function minimization problem. Additionally, two constraints directly determine the solution. These are trivial cases to solve. Thereby, little extra time complexity will be added to the problem.

The main computational burden in this work appears in solving the problem without constraints. As stated in the last part of Section 3.1, solving this case has similar complexity to H -infinity filter, but will be slower than Kalman Filter (EKF), hence also slower than Sliding Mode Observer (SMO). However, they just differ by a small constant scalar. On the other hand, the experimental time used for each method is summarised in Table 1. The

elapsed time is tiny as $0.2541ms$ per loop. Although the MPCO proposed in this paper is the slowest among the comparisons, it is yet fast enough for online application.

Filter Method	SMO	EKF	H -finity	MPCO
Elapsed Time (ms) per Loop	0.1062	0.1364	0.1456	0.2542

Table 1: Experimental Time Complexity Comparisons

3.4. Reconditioning Operation indicator

Substantial investigations on bench-scale and grid-scale ZNBs, have indicated that a periodic reconditioning operation (every 15/20 cycles) [13], i.e. discharging the ZNBs in a trickle current profile, would effectively reactivate the battery. By doing so, even after 3000+ cycles, ZNBs are still performing well [17]. However, little contribution has been made on identifying the reconditioning moment in the literature. In practice, frequent or premature recondition maintenance will lead to a waste of energy in the storage system, because the process of trickle discharging can last for more than a day. On the other hand, when ZNBs are cycling under the poor conditions, the chain reactions to damage the cell housing and electrodes catastrophically will be progressively provoked. The preliminary studies indicate that in poor operating conditions, ZNBs are subject to two main issues, which are anodes self-corrosion and cathodes transformation. The latter one specifically refers to active materials stripping and swelling. As a result, the effective reaction areas of electrode are not stable leading to the variations in capacity, and it will then deteriorate the accuracy of SoC estimate. In this paper, the developed MPCO enhances the robustness of estimates. In addition, the reversely calculated battery capacity through the SoC estimation has been selected as the reconditioning indicator.

Revisiting Eq.(14), the battery capacity can be interpreted by the ratio of accumulated coulomb, which is explained by the SoC change during a certain time.

$$Q = \frac{\eta \int_{t_\alpha}^{t_\beta} I_L dt}{SoC_{t_\beta} - SoC_{t_\alpha}} \quad (37)$$

where t_α and t_β are the starting and ending points of pre-defined time interval. It is worth noting that the robustness of SoC estimations i.e. SoC_{t_α} and SoC_{t_β} is essential to the capacity estimate. One key element has to be emphasized accordingly. The time intervals should be set sufficiently large to make SoC estimate converge. In this paper, t_α and t_β are prescribed as the 100 sample points after the start-up and 100 sample points ahead of the end-point, respectively. Therefore, underpinned by this framework, the multi-windows method is able to be implemented to improve the accuracy of the previous SoC estimations again, which will be elaborated in Section 5.3. The updated capacity after each discharging cycle will be employed as the reconditioning indicator to judge the health conditions of ZNBs. If the capacity suddenly drops below 90% of the nominal capacity, the ZNBs have to be stopped for maintenance.

3.5. The Framework of the Proposed Observer

In this paper, the RLS based online identification method is used to parameterize the time-varying system, i.e. the ECM model. Therefore, the effects of aging evolution and varying working conditions have been considered in the process of parameters identification. Afterwards, the identified parameters are applied to the proposed MPCO to obtain a robust SoC estimation. Then the capacity is updated at the end of a full cycle, which will be used as the base capacity in the following cycle to overcome the capacity fluctuation issues. The capacity estimate is regarded as an indicator for the reconditioning and maintenance. The systematic flowchart of the proposed method is given in Fig.2.

4. Experiments and Setups

4.1. Experimental Apparatus

Fig.3 illustrates the schematic of the experimental apparatus. A bench scale ZNBs demonstrator has been fabricated based on the previous studies [9, 11]. The designed capacity of this ZNBs demonstrator is $3.70Ah$. The operating flow rate is remaining at $19cm/s$ [9]. The battery tester *NEWARECT-3008W-15V3A* generates the testing current regimes on the ZNBs demonstrator. According to the specification of battery tester, the measurement

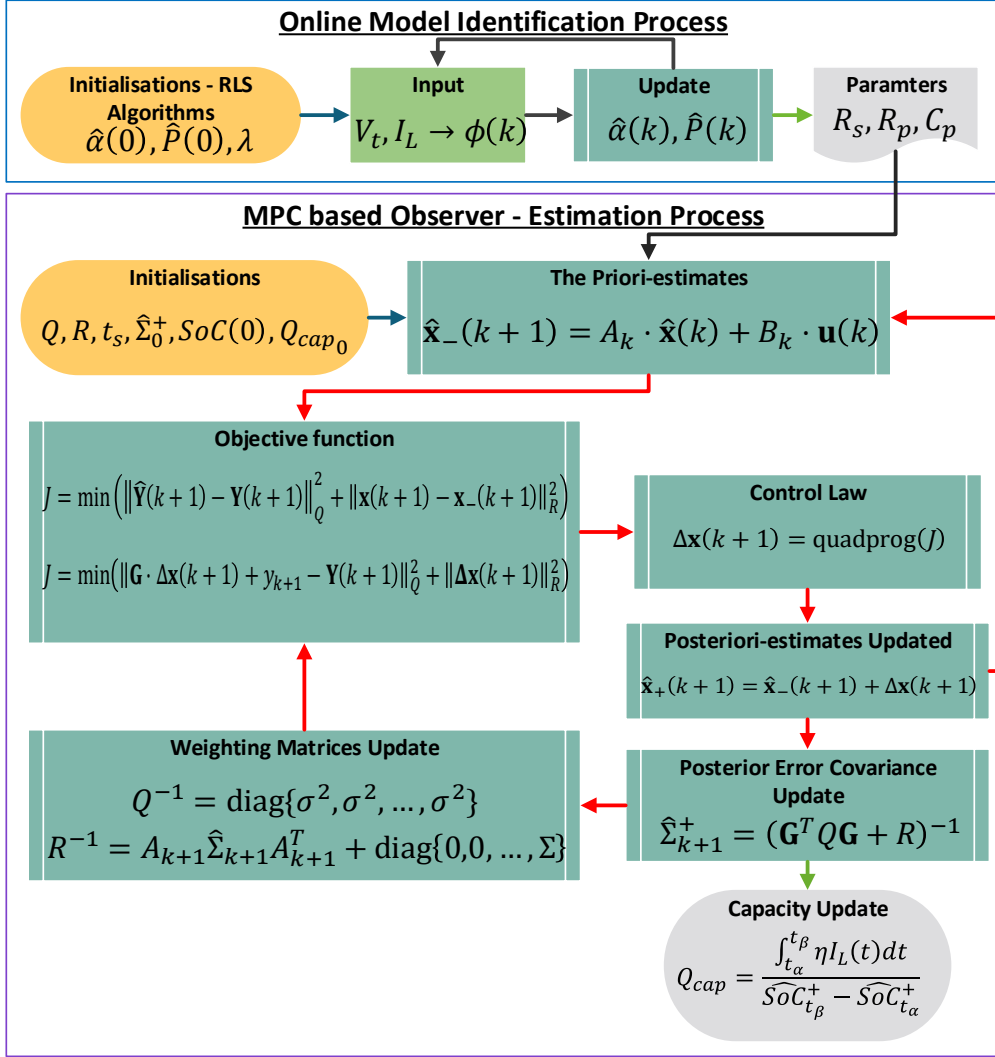


Figure 2: Implementation flowchart of the developed method

errors are bounded within 0.1%. Throughout the entire experiments, the room temperature maintains $25 \pm 3^\circ C$, and the output data will be logged by an external host computer. It is notable that the separators are not required in such a single flow system.

4.2. Pulse Tests

1C (3.70A) current stress is loaded into the ZNBs in pulses. Specifically, the charge and discharge regimes are a constant 10min pulse in a 1C current rate. In this work, the 1C current rate in pulse is dedicated to exciting the batteries in a moderate manner. Consequently,

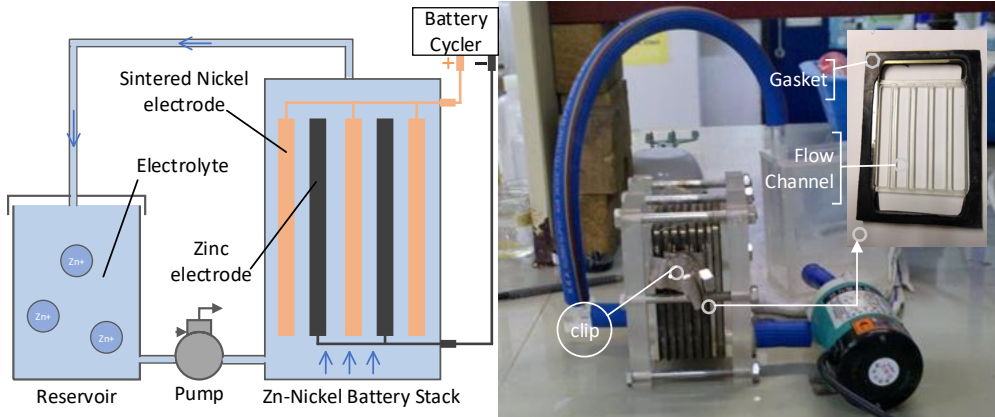


Figure 3: Schematic diagram and experimental apparatus

the applied pulse tests protect the unmaturred, hand-made ZNBs demonstrator from over-excitations and rapid deterioration. In particular, the battery rests for $15min$ after each pulse to secure the completeness and sufficiency of the redox reactions. On the other hand, the dynamic pulses tests are carried out as well, which reflect the responsive performance of the battery under the scenario of frequency control [32]. Four pulse patterns in terms of $1C$, $1.5C$, $0.5C$, and $1C$ are consecutively loaded into the battery during charge/discharge processes. The dynamic pulse tests are conducted under an acceptable current stress for short-term testing, aiming to examine the transient behaviours, convergence and tracking performance of the proposed model and observer, while preventing the demonstrator from over-excitation.

4.3. Capacity tests

Galvanostatic cycle tests [23] are carried out using the constant charge/discharge rates of $1C$ ($3.70A$). The objective of these tests is to manifest the effectiveness of the proposed method to handle the capacity fluctuation issues. In each cycle, the charging phase is terminated once the ZNBs demonstrator has reached its full capacity $3700mAh$. It is notable that the capacity calculation in this paper is based on the ability of nickel electrode. And then, the demonstrator is treated as fully discharged when the terminal voltage V_t drops to the cut-off voltage $1.2V$.

4.4. Applicability Tests

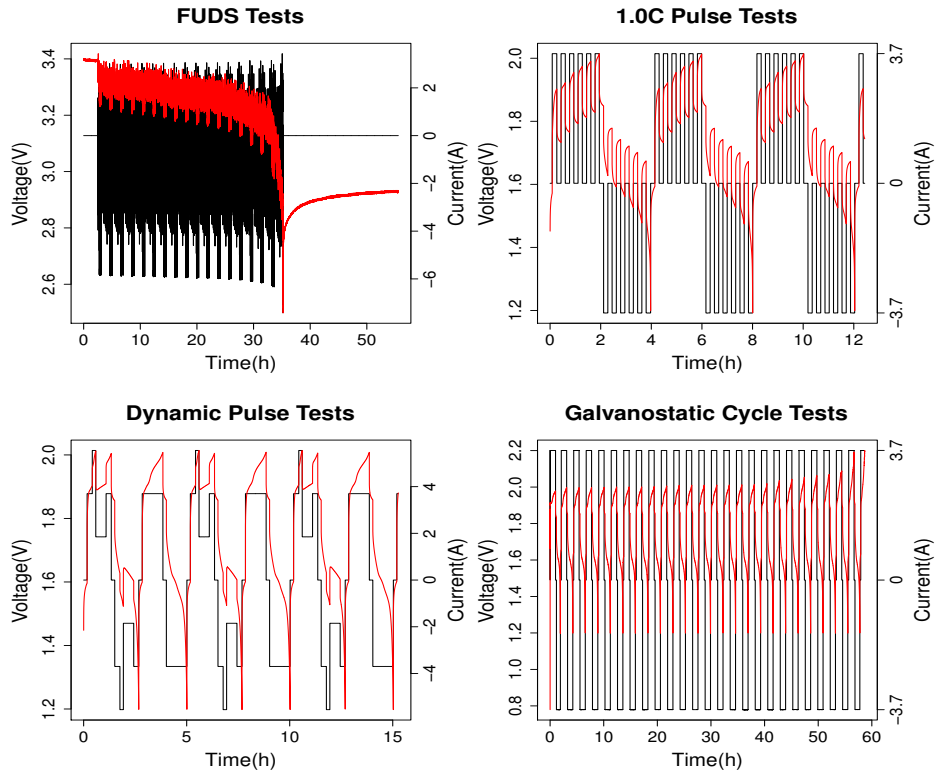
To further validate the generality of the proposed observer in more complex current profiles and deal with different electrochemical storage applications, the Federal Urban Driving Schedule (FUDS) test [23] is carried out on a $5Ah$ lithium battery to test the proposed method. The regime of FUDS satisfies the automobile industry standards. In addition, it represents the power requirements in the practical utilization of electric vehicle (EV). The FUDS test starts with a fully charged state under the CCCV charging mode, and the test is terminated by consuming all the net capacity.

Throughout each process of above tests, the reference SoC trajectory is obtained by the highly reliable CC method. Testing regimes are detailed in Fig.4(a), where the current profiles and voltage responses are depicted in black and red lines respectively.

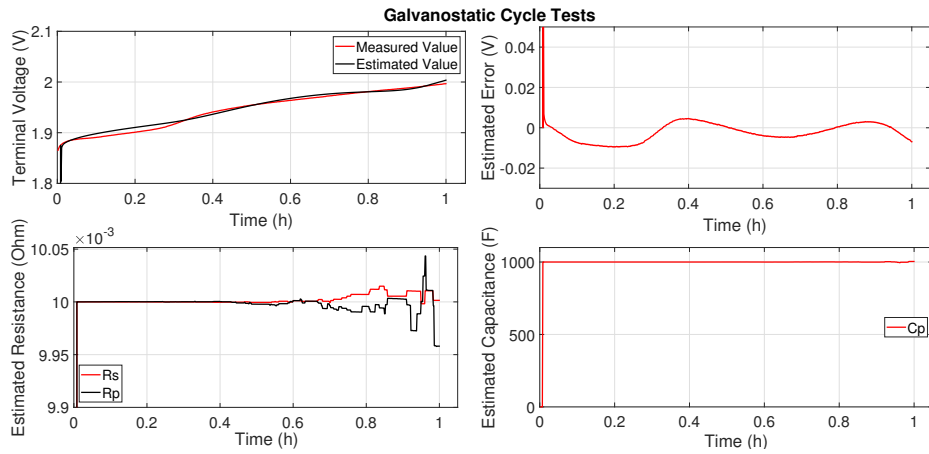
5. Experimental Results and Discussion

5.1. Model verification

The RLS based simple first-order ECM is used in this work to reproduce the battery dynamics under different working conditions. In order to verify the efficacy of the used first-order ECM battery model, one set of the modelling results of the RLS online model identification are given in Fig.4(b), in which a $1C$ ($3.7A$) constant current is imposed on the battery i.e. the Galvanostatic cycle tests. There is no prior information available for the model parameters. The parameters in ECM are thus erroneously initialized as $R_s = R_p = 0.02\Omega$ and $C_p = 1000F$. As depicted in the Fig.4(b), during the entire charging process, the output signals i.e. terminal voltage V_t highly match the input measured voltage, and the modelling errors are within $\pm 0.01V$. Though a reasonable deviation appears at the start-up stage because of the erroneous initialisation, the outputs converge to the voltage trajectory quickly. In addition, the parameters of electrical elements in the ECM encompassing R_s , R_p , and C_p converge in fast manners and keep stable throughout the charging phase, which are also in accord with the intrinsic features of the ZNBs acting as a slowly time-varying system.



(a) The details of the tests regimes



(b) RLS based online model identification

Figure 4: Detailing of the tests regimes and modelling performance

5.2. Accuracy of states estimates

In this paper, the dynamic pulse tests as shown in Fig.4(a) are carried out to mimic the practical RFBs working conditions introducing the intermittence of renewable electricity sources. Additionally, for the purpose to compare the performance of state estimates among different algorithms in terms of the SoC tracking performance, transient behaviours, estimation robustness, convergence. etc., a more complex excitation is imposed on the ZNBs, namely dynamic pulse tests as shown in the Fig.4(a). With an intentionally initial SoC error of -20% , the resultant SoC estimation of the proposed MPCO method is compared with the state-of-the-art algorithms such as EKF, H -infinity, and SMO. In order to conduct fair comparisons among all SoC estimators, the efforts on the parameters turning process, e.g. P , Σ , and σ . etc. are kept in a similar level, besides, it should be noted that the size of the decision window (horizon) is set as one to secure the approximate computational burden are used. The SoC estimation and comparisons are displayed in Fig.5.

From the observations on Fig.5(a) and Fig.5(b), the estimation of MPCO presents a good convergence behaviour to the SoC reference trajectory, resulting from the imposed hard constraints on the polarization voltage estimation V_p revealed in Fig.5(c). Specifically, as illustrated in the zoom-in plot of the starting stage, the SoC estimation provided by MPCO converges to the CC reference faster than other counterparts, while SMO shows the slowest convergence performance. The relative poor convergence is foreseeable in SMO, due to its simplest structural design. In this regard, the analytical discussion among different estimators are detailed in Section 6. Apart from the ending stage, the worst transient behaviours occurs in the first transient pulse, where the current changes from $1C$ to $1.5C$. It can be explained by the effects of the unstable model parameters in the initial stage. As shown in Fig.5(b), the estimation performances of EKF, H -infinity and SMO, are getting worse in the ending stage. The comparisons of SoC estimate error among these four approaches are detailed in Table.2, where the proposed MPCO method provides the best accuracy of the SoC estimation. Additionally, unlike the other counterparts, MPCO exhibits strong robustness, and the estimation accuracy of MPCO still remains stable yet, with the SoC estimation errors almost bounded within 1.5% . These phenomena are owing to the

introduced hard constraints on the polarization voltage V_p . As presented in Fig.5(c), the proposed MPCO method is capable of not only incorporating the priori-knowledge of the battery intrinsic electrochemical properties into SoC estimation, but also restricting the *SoC* estimation within reasonable region. Therefore, the SoC estimation is further optimised by the proposed MPCO method. On the other hand, the proposed MPCO inherits the advantages of MPC that are good at handling the non-Gaussian noises according to Eq.(14) and Eq.(15). In this paper, for the convenience sake, only the Gaussian noises with a standard deviation of $10mV$ is imposed on the voltage measurement for all the SoC estimators. Moreover, the accuracy of capacity estimation will be enhanced by raising the length of the windows, as discussed in the following content 5.3.

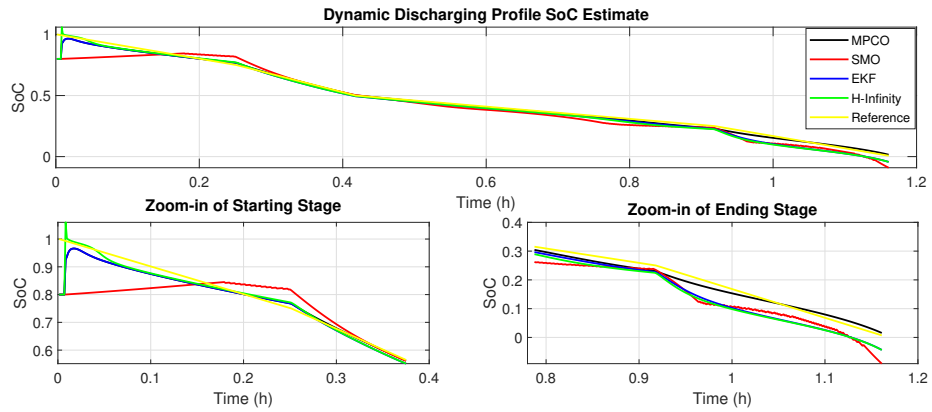
SoC Error	MPCO	SMO	EKF	H-Infinty
Mean	-0.0087	-0.0314	-0.0227	-0.0225
Std. Dev.	0.0187	0.0458	0.0229	0.0250

Table 2: Dynamic Charging Profile SoC Estimate Error Summary

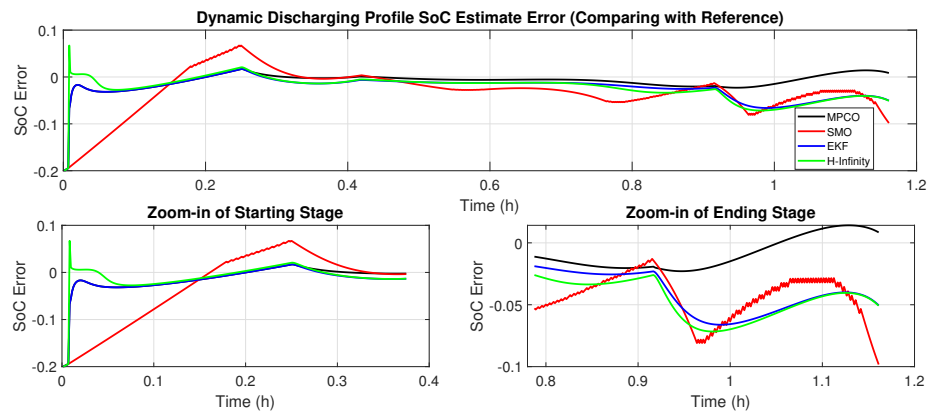
5.3. Capacity estimation and effects of windows sizes

A major objective of the proposed MPCO is to estimate capacity dynamically then determine the time for reconditioning. Thereby, the estimated capacity is expected to be an indicator for the maintenance of ZNBs. The proposed MPCO is applied for the SoC estimation over the galvanostatic cycling tests as depicted in Fig.4(a). In this section, in order to obtain a robust estimation of capacity, different horizon window of the state variable are tested. Furthermore, the effects of window size are discussed.

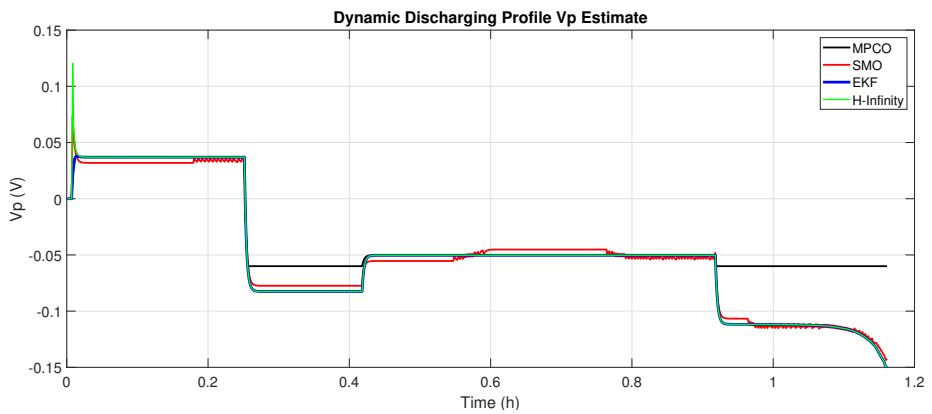
Fig.6(a) concludes the resultant SoC estimates over 15 discharging cycles. Large error spikes only occur at the starting stage of each discharging cycle, due to the intentional -20% SoC initialization error. However, all the applied methods attenuate the initial errors and converge quickly. Through comparison with EKF in Fig.6, MPCO has remarkably outperformed in the SoC estimation. In this regard, as the number of cycling increases,



(a) SoC estimations under different filter designs

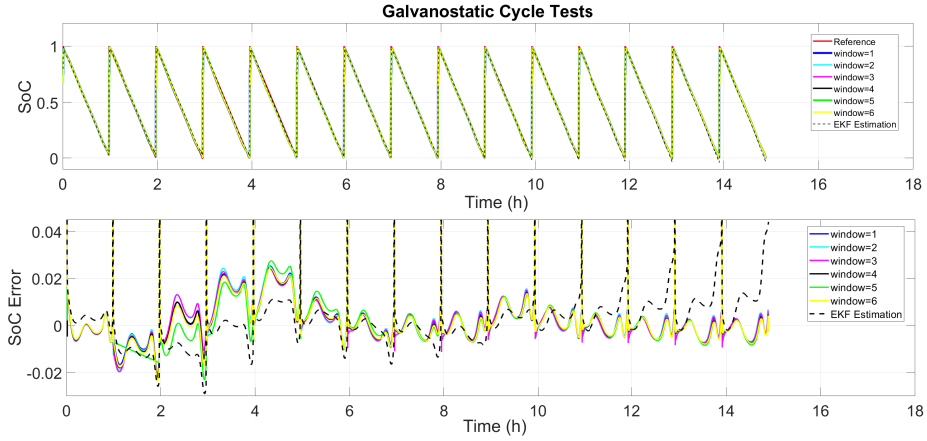


(b) Error of Soc estimation under different filter designs

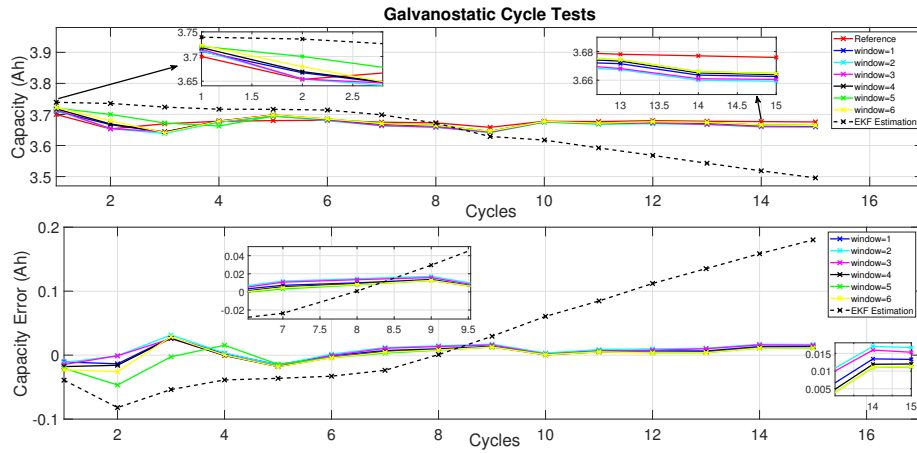


(c) Polarization voltage V_p estimations under different filter designs

Figure 5: The states estimation results and comparisons during the dynamic pulse tests



(a) SoC estimation under different windows



(b) Capacity estimation under different windows

Figure 6: Capacity estimation and effects of windows sizes during the galvanostatic cycling tests

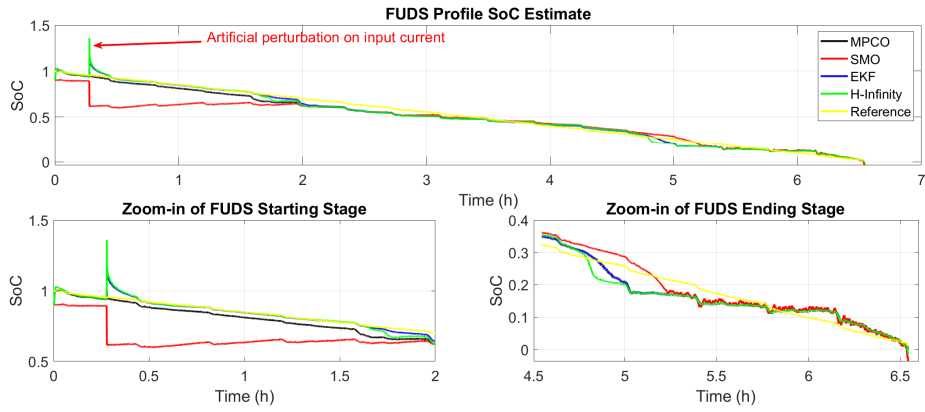
the SoC estimations provided by EKF are going far from the CC references, where larger discrepancies can be observed after 10 cycles. These phenomena can be explained from two aspects. Firstly, even single window MPCO outperforms EKF due to the constraints in SoC estimation. At the start of each cycle, an intentional SoC initialization error is considered. The SoC constraints help in faster convergence and prevent underestimation (below 0) at the end of each cycle. While EKF is tend to underestimate SoC when approaching later cycles (from 11 to 15) due to weak traceability of battery capacities. The underestimation of SoC then results in poorer capacity estimates as detailed in Fig.6(b). With the constraints in the

proposed MPCO, this cross-interference can be more manageable. Secondly, as illustrated in Fig.6(b), longer window outperforms in the convergence speed of the capacity estimation. For instance, when the window length increases to 6, the capacity estimate converges to the reference value quickly, bringing the estimation error down to tiny values, merely after 1 cycle. As interpreted by Eq.(24), in the process of solving objective function, more previous measurements are involved in the optimization when longer windows are used. Consequently, the past SoC estimates are updated as well, becoming closer to the SoC-OCV table. Except for the faster convergence speed, the performance of these counterparts (window lengths from 1 to 6) is comparable and outperforms traditional EKF, which is foreseeable as explained in previous context. Throughout the entire 15 discharging cycles, the estimation errors of the capacity are subtle, only within $\pm 2\%$. According to Eq.(37), the accurate estimation of SoC thus reinforces the precision of capacity estimates accordingly. The simulation results further verify the effectiveness of the proposed MPCO method as given in Fig.6. Therefore, the proposed MPCO is able to reflect the dynamics of the practical capacity, which is poised to be a good indicator to determine the moment of reconditioning.

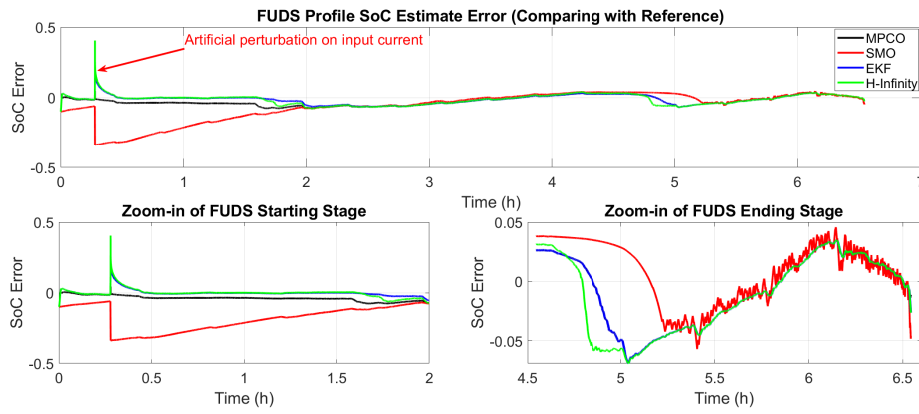
5.4. Validation of applicability

In order to test the generality of the proposed MPCO, a 5Ah prismatic *LiFePO4*-Graphite lithium battery (GWL/Power Company) has been tested. Throughout the entire tests, the same initial settings in the above Section 5.1 and Section 5.2 are adopted on EKF, H -infinity, and SMO approaches as well. The SoC and polarization voltage V_p are restricted within 0 to 1 and $\pm 0.04V$, respectively. The FUDS testing profile, given in the Fig.4(a), is loaded to the lithium battery with the erroneously initial SoC value of -20% . According to the aforementioned, the length of the decision window is set as 1 to provide a short-term comparison of SoC estimation among different SoC estimators. In addition, at the early stage of FUDS tests, an artificial perturbation, 10A charging current lasts for 5s, is intentionally inserted in the input current to evaluate the robustness of the proposed methods.

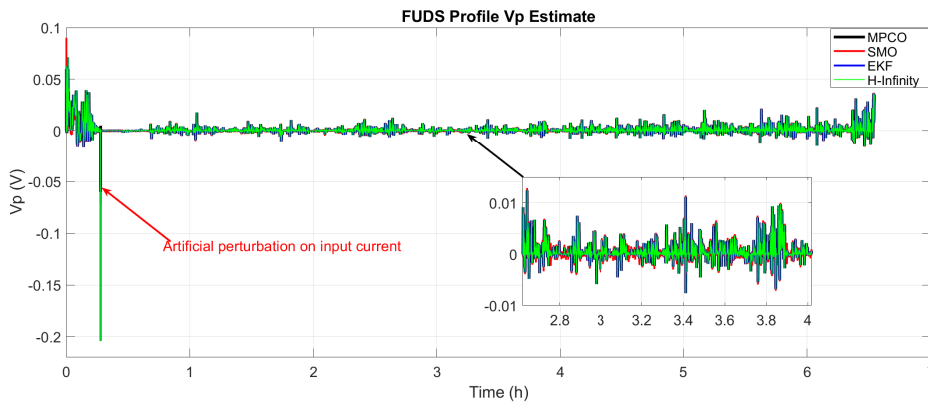
As shown in Fig.7, all the estimators attempt to attenuate the initial errors in a fast man-



(a) SoC estimations under different filter designs



(b) Error of Soc estimation under different filter designs



(c) Polarization voltage V_p estimations under different filter designs

Figure 7: The states estimation results and comparisons during FUDS tests

ner. As shown in the zoom-ins in Fig.7(a), before the artificial perturbation, the SoC estimation converge to the reference value fast. Yet, a slower convergence speed can be observed on SMO, which is in accordance with the ZNBs tests. In other words, EKF, H -infinity and the proposed MPCO give similar estimation accuracy and convergence speed. Afterwards, an artificial perturbation in the charging current with a pulse form of $100A$ magnitude is imposed on the input signals at $t = 1000s$. Due to the prescribed constraints on the internal states in the observer design, the proposed MPCO method outperforms among all four approaches, showing up the best performance of disturbance rejecting and robustness. We believe these phenomena are owing to the imposed estimation constraints, which limit the state estimation in a reasonable range and reduce the estimation errors. Additionally, Fig.7(b) reveals that SMO provides the worst performance in terms of robustness and convergence at the starting stage, in which the convergence speed can be adjusted by the prescribed value of error covariance. Typically, a large value can converge more quickly, but it will also bring ripples to the SoC estimation, losing the accuracy. However, as depicted in Fig.7(b) the error of SoC estimation will remarkably increase when the discharging phase is approaching the end and the terminal voltage is close to the cut-off voltage. It is because of the progressive nonlinearity of SoC-OCV table in the range of lower SoC. In this regard, the utilized first-order ECM is not able to capture the battery dynamics anymore, leading to equally poor performance of MPCO, EKF and H-infinity. However, the primary goal of MPCO to comply with the intrinsic electrochemical properties has still been achieved as depicted in Fig.7(c). Based on Eq.(31) and Eq.(32), the hard constraints are imposed on the polarization voltage and SoC. All the estimated V_p are thus bounded within the empirical value $\pm 0.04V$, which pre-filters out the interference of estimation outliers, leading to more accurate estimation of V_p . It is worth noting that the MPCO provides potential ways to leverage the electrochemical knowledge of batteries. If more explicit constraints can be prescribed, in principle, the accuracy of SoC estimation can be increased significantly through the proposed MPCO scheme. The simulation results verify the applicability of the proposed method on other electrochemical systems. In specific, the proposed MPCO performs competitively on the SoC estimation for lithium batteries, even more effectively in the

convergence speed. Additionally, the robustness of the proposed method is stronger than other counterparts.

6. Analytical Comparisons among Different Estimators

This section provides a brief analytical comparison among the four different online SOC estimators mentioned in this paper. Starting with the simplest and fastest method, namely Sliding Mode Observer (SMO), this observer updates the state vector estimate according to measurement equation by:

$$x^+(k) = x^-(k) + \begin{cases} g_1, & f(x^-(k), u(k)) > y(k) \\ g_2, & f(x^-(k), u(k)) < y(k) \end{cases}$$

where g_1 and g_2 satisfy

$$\begin{cases} g_1^T \frac{\partial f}{\partial x} < 0, & f(x, u(k)) > y(k) \\ g_2^T \frac{\partial f}{\partial x} > 0, & f(x, u(k)) < y(k) \end{cases}$$

Due to the simple structure, the advantages of SMO are obvious. It is straightforward to be utilised, and thus has the smallest computational burden. Furthermore, the updating step vector g_1 and g_2 are easy to find. On the other hand, the disadvantages of SMO are apparent as well. The most unbearable one is that the arbitrary selection for g_1 and g_2 might result in poor convergence, which has been reflected in the aforementioned simulation.

To overcome the drawbacks of SMO, the Kalman Filter/Extended Kalman Filter (EKF) acts as an advanced method which maintains the basic logic on sliding of SMO, but further introduces the covariance matrix of the state vector. The Kalman gain has secured the sliding requirements on g_1 and g_2 in SMO:

$$\begin{aligned} K_k &= P_{k|k-1} C_k^T (C_k P_{k|k-1} C_k^T + \Sigma_\nu)^{-1} \\ x^+(k) &= x^-(k) + K_k e_k = x^-(k) + g_k \\ e_k^T C_k g_k &= e_k^T C_k K_k e_k = e_k^T C_k P_{k|k-1} C_k^T (C_k P_{k|k-1} C_k^T + \Sigma_\nu)^{-1} e_k \\ &= e_k^T C_k P_{k|k-1} C_k^T e_k (C_k P_{k|k-1} C_k^T + \Sigma_\nu)^{-1} > 0 \end{aligned}$$

The KF estimation aims at acquiring state estimate with the smallest covariance matrix, i.e. any linear combination of state variables with the smallest variance. By doing this KF exhibits the fastest convergence.

However, Kalman Filter also shows its limitations. The most widely argued point is the assumption that errors follow normal distributions. This priori knowledge is not applicable to most cases in the real world. In order to solve this issue, the H -infinity filter has been proposed. Comparing with Kalman Filter, the H -infinity filter has the following gain value and covariance matrix update:

$$\begin{aligned}\hat{S}_k &= L_k^T S_k L_k \\ P_{k|k} &= P_{k|k-1} \left(I - \theta \hat{S}_k P_{k|k-1} + C_k^T \Sigma_\nu^{-1} C_k P_{k|k-1} \right)^{-1} \\ K_k &= P_{k|k} C_k^T \Sigma_\nu^{-1}\end{aligned}$$

The H -infinity is only interested in the user-defined linear combination of state variables, i.e. $L_k x(k)$. Another difference from KF is in user-defined “enlarge” parameter, which makes the covariance matrix and gain value slightly larger than in KF, intentionally leading to a more robust result at the expense of larger covariances. In addition, it can be verified with simple algebra that under special case of chosen parameters, H -infinity is equivalent to KF.

Nevertheless, all three methods discussed above cannot cope with constraints issues. The method proposed in this paper is based on MPC framework to induce constrained estimates. It can also be shown that without constraints, the performance of MPCO is equivalent to the KF, which has further guaranteed the correctness of the rationale behind the proposed MPCO method. Besides, MPCO is easy to understand and readily implementable.

7. Conclusion

This paper develops a novel SoC estimation method based on the powerful **optimization tool**, namely, MPCO. Additionally, an in-depth investigation of the emerging grid-tied battery technique ZNBs has been provided in this work. The RLS method is incorporated with a widely accepted first-order ECM for the parameter identification, which provides a simple

implementation of ZNBs modelling not only to ensure the accuracy but also to simplify the battery model structure. Moreover, there are two major advantages of the proposed observer. Firstly, based on the inherent electrochemical knowledge, state constraints are incorporated into the estimation process, which brings more robust estimates. Secondly, an attempt in multi-window framework has demonstrated better performance in capacity estimation. The experiments and simulations have verified the convergence, effectiveness, and the generality of the proposed MPCO approach. Underpinned by the advantages of the proposed MPCO, this method can provide a robust and reliable estimate to ZNBs capacity, with a good tracking behaviour to handle the fluctuating capacity issues. This estimated capacity can be regarded as an indicator of the reconditioning maintenance. Additionally, the relationships among the state-of-the-art estimators has been discussed briefly in this work.

References

- [1] K. Divya, J. Østergaard, Battery energy storage technology for power systems—an overview, *Electric Power Systems Research* 79 (4) (2009) 511–520.
- [2] P. J. Hall, E. J. Bain, Energy-storage technologies and electricity generation, *Energy policy* 36 (12) (2008) 4352–4355.
- [3] S. Vazquez, S. M. Lukic, E. Galvan, L. G. Franquelo, J. M. Carrasco, Energy storage systems for transport and grid applications, *IEEE Transactions on Industrial Electronics* 57 (12) (2010) 3881–3895.
- [4] P. Leung, X. Li, C. P. De León, L. Berlouis, C. J. Low, F. C. Walsh, Progress in redox flow batteries, remaining challenges and their applications in energy storage, *Rsc Advances* 2 (27) (2012) 10125–10156.
- [5] A. Z. Weber, M. M. Mench, J. P. Meyers, P. N. Ross, J. T. Gostick, Q. Liu, Redox flow batteries: a review, *Journal of Applied Electrochemistry* 41 (10) (2011) 1137.
- [6] B. Li, J. Liu, Progress and directions in low-cost redox-flow batteries for large-scale energy storage, *National Science Review* 4 (1) (2017) 91–105.
- [7] C. P. De Leon, A. Frías-Ferrer, J. González-García, D. Szánto, F. C. Walsh, Redox flow cells for energy conversion, *Journal of Power Sources* 160 (1) (2006) 716–732.
- [8] M. Skyllas-Kazacos, M. Rychcik, R. G. Robins, A. Fane, M. Green, New all-vanadium redox flow cell, *Journal of the Electrochemical Society* 133 (1986) 1057.
- [9] J. Cheng, L. Zhang, Y.-S. Yang, Y.-H. Wen, G.-P. Cao, X.-D. Wang, Preliminary study of single flow zinc–nickel battery, *Electrochemistry Communications* 9 (11) (2007) 2639–2642.

- [10] B. S. Kwak, D. Y. Kim, S. S. Park, B. S. Kim, M. Kang, Implementation of stable electrochemical performance using a $\text{Fe}_0.01\text{ZnO}$ anodic material in alkaline Ni–Zn redox battery, *Chemical Engineering Journal* 281 (2015) 368–378.
- [11] L. Zhang, J. Cheng, Y.-s. Yang, Y.-h. Wen, X.-d. Wang, G.-p. Cao, Study of zinc electrodes for single flow zinc/nickel battery application, *Journal of Power Sources* 179 (1) (2008) 381–387.
- [12] Y. Im, J. Kim, K. S. Park, T. W. Cho, J. Jeon, K.-i. Chung, K. Eguchi, M. Kang, Influence of small amount of Mg incorporated into hexagonal ZnO crystal on cell performance in membrane free zinc–nickel redox battery, *Journal of Industrial and Engineering Chemistry*.
- [13] Y. Ito, M. Nyce, R. Plivelich, M. Klein, D. Steingart, S. Banerjee, Zinc morphology in zinc–nickel flow assisted batteries and impact on performance, *Journal of Power Sources* 196 (4) (2011) 2340–2345.
- [14] B. S. Kwak, S. W. Jo, K. S. Park, T. W. Cho, J. Jeon, K.-i. Chung, M. Kang, Synthesis of microcrystalline ZnO as an anodic material via a solvothermal method, and its electrochemical performance in Ni/Zn redox battery, *Journal of Industrial and Engineering Chemistry* 46 (2017) 111–118.
- [15] J. Kim, Y. Im, K. S. Park, T. W. Cho, J. Jeon, K.-i. Chung, M. Kang, Improved cell performances in Ni/Zn redox batteries fabricated by ZnO materials with various morphologies synthesized using amine chelates, *Journal of Industrial and Engineering Chemistry* 56 (2017) 463–471.
- [16] Y. Yuan, J. Tu, H. Wu, Y. Li, D. Shi, X. Zhao, Effect of ZnO nanomaterials associated with Ca(OH)₂ as anode material for Ni–Zn batteries, *Journal of Power Sources* 159 (1) (2006) 357–360.
- [17] D. E. Turney, M. Shmukler, K. Galloway, M. Klein, Y. Ito, T. Sholklapper, J. W. Gallaway, M. Nyce, S. Banerjee, Development and testing of an economic grid-scale flow-assisted zinc/nickel-hydroxide alkaline battery, *Journal of Power Sources* 264 (2014) 49–58.
- [18] M. Morari, J. H. Lee, Model predictive control: past, present and future, *Computers & Chemical Engineering* 23 (4-5) (1999) 667–682.
- [19] J. H. Lee, Model predictive control: Review of the three decades of development, *International Journal of Control, Automation and Systems* 9 (3) (2011) 415.
- [20] J. Zhang, Y. Zhou, Y. Li, G. Hou, F. Fang, Generalized predictive control applied in waste heat recovery power plants, *Applied Energy* 102 (2013) 320–326.
- [21] M. G. Forbes, R. S. Patwardhan, H. Hamadah, R. B. Gopaluni, Model predictive control in industry: Challenges and opportunities, *IFAC-PapersOnLine* 48 (8) (2015) 531–538.
- [22] X. Hu, S. Li, H. Peng, A comparative study of equivalent circuit models for Li-ion batteries, *Journal of Power Sources* 198 (2012) 359–367.
- [23] U. ABC, US ABC electric vehicle battery test procedures manual, revision 2, principal author: Gary Hunt, Idaho National Engineering Laboratory (INEL), US Department of Energy Idaho Field Office, DOE/ID-10479, Rev 2.

- [24] Z. Wei, K. J. Tseng, N. Wai, T. M. Lim, M. Skyllas-Kazacos, Adaptive estimation of state of charge and capacity with online identified battery model for vanadium redox flow battery, *Journal of Power Sources* 332 (2016) 389–398.
- [25] G. L. Plett, Extended kalman filtering for battery management systems of lipb-based hev battery packs: Part 3. state and parameter estimation, *Journal of Power sources* 134 (2) (2004) 277–292.
- [26] R. Xiong, Q. Yu, L. Y. Wang, C. Lin, A novel method to obtain the open circuit voltage for the state of charge of lithium ion batteries in electric vehicles by using h infinity filter, *Applied Energy* 207 (2017) 346–353.
- [27] R. Xiong, Y. Zhang, H. He, X. Zhou, M. G. Pecht, A double-scale, particle-filtering, energy state prediction algorithm for lithium-ion batteries, *IEEE Transactions on Industrial Electronics* 65 (2) (2018) 1526–1538.
- [28] I.-S. Kim, Nonlinear state of charge estimator for hybrid electric vehicle battery, *IEEE Transactions on Power Electronics* 23 (4) (2008) 2027–2034.
- [29] Y. Wang, H. Fang, Z. Sahinoglu, T. Wada, S. Hara, Adaptive estimation of the state of charge for lithium-ion batteries: Nonlinear geometric observer approach, *IEEE Transactions on Control Systems Technology* 23 (3) (2015) 948–962.
- [30] S. Dey, B. Ayalew, P. Pisu, Nonlinear robust observers for state-of-charge estimation of lithium-ion cells based on a reduced electrochemical model, *IEEE Transactions on Control Systems Technology* 23 (5) (2015) 1935–1942.
- [31] C. Zou, A. Klintberg, Z. Wei, B. Fridholm, T. Wik, B. Egardt, Power capability prediction for lithium-ion batteries using economic nonlinear model predictive control, *Journal of Power Sources* 396 (2018) 580–589.
- [32] U. International Electrotechnical Commission, Iec 61427-2 secondary cells and batteries for renewable energy storage â general requirements and methods of test â part 2: On-grid applications, *International Standards and Conformity Assessment for all electrical, electronic and related technologies*.